Journal of Molecular Structure 1223 (2020) 128984

Contents lists available at ScienceDirect

Journal of Molecular Structure

journal homepage: www.elsevier.com/locate/molstr

Synthesis, spectral characterization, quantum chemical calculations, thermal studies and biological screening of nitrogen and oxygen donor atoms containing Azo-dye Cu(II), Ni(II) and Co(II) complexes

Asma A. Alothman*, Munirah D. Albaqami, Razan A. Alshgari

Department of Chemistry, College of Science, King Saud University, P.O. Box 22452, Riyadh 11495, Saudi Arabia

ARTICLE INFO

Article history:
Received 27 May 2020
Revised 24 July 2020
Accepted 26 July 2020
Available online 27 July 2020

Keywords:
Azo-dye complexes
Spectral
Thermal
Antioxidant
Cytotoxic
Quantum chemical calculations

ABSTRACT

Present research work focuses on the synthesis of novel azo-dye Cu(II), Ni(II) and Co(II) chelates of Schiff base based ligand having antimicrobial activities. Azo-dye Cu(II) and Zn(II) complexes derived 7-benzyl-4-(phenyldiazenyl)quinolin-8-ol (HBPDQ) was obtained and described by spectroscopic tools and TGA analysis. UV-visible, IR, ^{1}H, ^{13}C & ^{15}N NMR spectra revealed that the HBPDQ uses its quinoline nitrogen ring and deprotonated hydroxyl group in coordination with Cu(II), Ni(II) and Co(II) ions. The Cu(II), Ni(II) and Co(II) chelates were predicted to be not electrolytic from the measured molar conductance values. Thermal properties and decomposition kinetics of the metal chelates are investigated using Coats-Redfern method. Magnetic susceptibility and electronic spectral data as well as quantum chemical calculations reveal the Cu(II), Ni(II) and Co(II) complexes are octahedral geometry. DFT studies revealed that geometries of metal complexes and azo-dye (HBPDQ) were entirely optimized in relation to use energy by 6-31+g (d,p) basis set. The kinetic parameters like activation energy (E^*), pre-exponential factor (A) and entropy of activation (ΔS^*) were quantified. Results of spectral studies of mass and TGA data confirmed the octahedral geometry for all chelates. The Cu(II), Ni(II) and Co(II) chelates were investigated for biological action against pathogenic fungi (*C. krusei, C. albican*) and bacteria (*S. aureus, E. coli*). The antimicrobial results confirmed that Cu(II), Ni(II) and Co(II) chelates possessed superior inhibition potential than the parent ligand (HBPDQ). The enhanced antimicrobial activity might be due to the chelation.

1. Introduction

Now days, the need for novel antimicrobial drugs has become significant due to the increased clinical and microbiological resistance of microbes. The biological applications of transition metal azo-dye have been reported long year back [1-6]. Azo-dye are –N=N– based compounds which after the formation of complex with a transition metal, demonstrate a wide range of biological and pharmacological activities [7]. These activities of the azo-dyes attracted a number of researchers and scientists to develop more novel azo-dyes based coordination complexes having enhanced antimicrobial properties [8-10]. These coordination compounds resulting after the interaction of metal cations with azo-dyes ligand, are acting as chelate. The number of donor atoms in the ligand further enhances the coordination sites providing more options for complexation [11-19]. The delocalization is enhanced after coordination to a metallic center. Generally, azo-dyes possess the different number of donor atoms and depending upon the donor atoms ligand behaves as monodentate, bidentate or tridentate in nature. The different metal complexes of azo-dyes demonstrate antimicrobial [17-19], anticancer [20-23], antitumor [24], antituberculosis [25], antioxidant [26], anti-HIV [27], anti-inflammatory [28], antileishmanial activities [29], antiviral [30], antiproliferative [31] and many more activities [32,33]. These ligands show excellent catalytical activities [34,35] significant mushroom tyrosinase inhibition action [36-37] used as precursors for nano-metal oxides [38,39]. The present paper reports the synthesis, characterization and theoretical studies of chloride salts of nano-sized Cu(II), Ni(II) and Co(II) chelates of 7-benzyl-4-(phenyldiazenyl)quinolin-8-ol (HBPDQ) ligand. The biological activities of the chelates were carried out and compared with the ligand and standard known drugs. The structural characterization was achieved applying the alternative analytical and spectral tools. Structural elucidation of the target complexes has been confirmed *via* molecular modeling studies.

* Corresponding author.

https://doi.org/10.1016/j.molstruc.2020.128984
0022-2860/

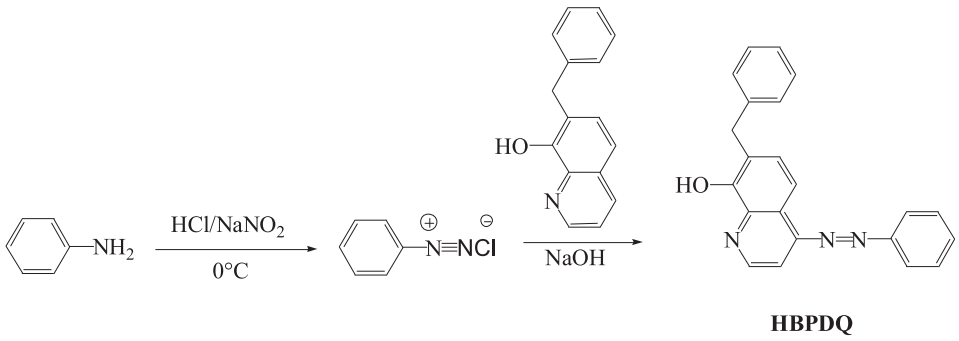

Scheme 1. The preparation of HBPDQ.

2. Experimental

2.1. Instrumentation and materials

Electronic spectra were conducted on a Unicam UV-Vis Spectrophotometer. Furthermore, readings of IR spectra were obtained on a Mattson 5000 FTIR spectrophotometer in a solid state. Measurements obtained via Sherwood balance determined magnetic susceptibilities at room temperature. Additionally, the ^{1}H NMR spectrum of HBPDQ was measured after addition of one drop of CD3OD to identify the signal of OH proton. ^{13}C NMR spectrum of HBPDQ was also recorded at the operating frequency 75 MHz and accordingly, chemical shifts were presented relative to TMS (tetramethylsilane). Perkin Elmer CHN Analyzer 2400 was used to estimate elemental analysis with deuterated organic solvents and TWS being utilized as an internal standard. Moreover, standard methods facilitated the calculations of M% in the chelates [39]. Jeol-300 MHz EPR spectrometer was employed to find the value of the copper complex electron paramagnetic resonance spectrum. Furthermore, TGA and DTA (20–1000°C) were obtained at a nitrogen flow rate under 20 ml/min and a heating rate of 15°C/min on a DTG-50 Shimadzu analyzer. Soon after, the room temperature molar conductivity of the complexes in DMSO solution (10^{-3} M) was measured using a deep vision 601 model digital conductometer. Additionally, the X-band EPR spectrum was performed at LNT (77 K) using TCNE as the g-marker and XRD (X-ray diffraction) patterns of the samples were recorded with a Rigaku Geiger flex X-ray diffractometer and all the diffraction patterns were obtained using CuKα_1 radiation, with a graphite monochromator at 5°/min scanning rate.

2.2. Synthesis of 7-benzyl-4-(phenyldiazenyl)quinolin-8-ol (HBPDQ)

In this method, aniline (1.00 g, 0.01 mol) was dissolved in acidic distilled water (10 ml of water containing 1.47 ml of 12 M (0.03 mol) conc. HCl). The temperature of the obtained solution was decreased to −5°C while stirring. A cold solution containing 0.689 g (0.01 mol) of $NaNO_2$ was poured dropwise into this solution to form the diazonium chloride. The obtained solution was then slowly poured into NaOH solution (0.01 mol) containing 2.35 g of 7-benzylquinolin-8-ol. The coloured product, which started to appear during addition, was preserved in an ice bath with stirring for 2 h. The precipitate was then separated by filtration, rinsed with deionized water and finally dried in a vacuum desiccator over anhydrous calcium chloride (Scheme 1).

2.3. Synthesis of Cu(II) Ni(II) and Co(II) complexes

The Cu(II) Ni(II) and Co(II)complexes were obtained by mixing 0.01 M of $CuCl_2.2H_2O$/ $NiCl_2.6H_2O$/$CoCl_2$. $6H_2O$ with 0.01 M of HBPDQ in ethanol (30 ml). The mix were refluxed at 60°C for ~ 5 h. The solid complexes were filtered then washed, recrystallized and dried in a vacuum.

Yield for **$[Cu(BPDQ)_2(H_2O)_2].2H_2O$**; **{$C_{44}H_{40}N_6O_6Cu$)} (1)**: 58 %; M.Wt.= 812.4; pale brown; analysis calc. C, 65.05; H, 4.96; N, 10.35; Cu, 7.82. Found: C, 64.97; H, 4.93; N, 10.26; Cu, 7.68. FT-IR (KBr, cm^{-1}): 3457 ν(O–H), H_2O; 1573 ν(C=N); 585 ν(Cu-O); 447 ν(Cu-N). UV-vis (λmax, nm, DMSO): 423, 684. Λ_m ($\Omega^{-1}cm^2mol^{-1}$): 6.54. μ_{eff} spin only (B.M.) = 1.83.

Yield for **$[Ni(BPDQ)_2(H_2O)_2].3H_2O$; {$C_{44}H_{42}N_6O_7Ni$} (2)**: 63 %; M.Wt.= 825.5; pale green; analysis calc. C, 64.02; H, 5.13; N, 10.18; Ni, 7.11. Found: C, 63.96; H, 5.03; N, 10.02; Ni, 7.03. FT-IR (KBr, cm^{-1}): 3375 ν(O–H), H_2O; 1580 ν(C=N); 581 ν(Ni-O); 445 ν(Ni-N); 419 ν(Ni-Cl). UV-vis (λmax, nm, DMSO): 448, 608, 912. Λ_m ($\Omega^{-1}cm^2mol^{-1}$): 5.21. μ_{eff} spin only (B.M.) = 2.82.

Yield for **$[Co(BPDQ)_2(H_2O)_2].3H_2O$; {$C_{44}H_{42}N_6O_7Co$} (3)**: 65 %; M.Wt.= 825.8; dark blue; analysis calc. C, 64.00; H, 5.13; Co, 7.14; N, 10.18. Found: C, 63.87; H, 5.12; Co, 7.03; N, 10.11. FT-IR (KBr, cm^{-1}): 3382 ν(O–H), H_2O; 1579 ν(C=N); 583 ν(Ni-O); 445 ν(Ni-N). UV-vis (λmax, nm, DMSO): 449, 614, 917. Λ_m ($\Omega^{-1}cm^2mol^{-1}$): 6.85. μ_{eff} spin only (B.M.) = 3.88.

2.4. Computational details

The calculations using DMOL3 program were performed in Materials Studio package [40], which is designed for the realization of large-scale density functional theory (DFT) calculations. DFT semi–core pseudo pods calculations (dspp) were performed with the double numerical basis sets plus polarization functional (DNP). The DNP basis sets are of comparable quality to 6–31G Gaussian basis sets [41]. Delley et al. showed that the DNP basis sets are more accurate than Gaussian basis sets of the same size [42]. The RPBE functional [43] is so far the best exchange–correlation functional [44], based on the generalized gradient approximation (GGA), is employed to take account of the exchange and correlation effects of electrons. The geometric optimization is performed without any symmetry restriction.

2.5. Biological evaluation - Antifungal & antibacterial activities

In vitro antibacterial and antifungal activities of the ligand and complexes were evaluated by Well diffusion method. The stock solutions of four different concentrations i.e., 250 ppm, 500 ppm, 750 ppm and 1000 ppm were prepared in DMSO. 28 g Nutrient Agar (NA) and 65 g Sabround Dextrose Agar (SDA) in 1 L of distilled water were used as medium to investigate antibacterial and antifungal activities, respectively. The SDA and distilled water mixture was heated and stirred properly to form uniform solution. This solution is autoclaved at 121°C for 15 min. The prepared media is poured in petri dishes (90 mm diameter) and kept for solidification. 4 wells (4 mm diameter) were cut out from the solidified media *via* sterile cork. The tested fungi in suspension form, spreader

on the agar surface and the different concentration solution (250, 500, 750, 1000 ppm) of tested compounds were filled in separate well. The petri dishes were sealed and kept for 2-3 hours for the diffusion of tested compounds at low temperature. Finally, the dishes were incubated for 24 hours at 27°C. The diameter of inhibition zone (mm) were measured and compared. The same abovementioned procedure has been adopted to evaluate antibacterial activities. The antifungal action of the compounds was tested for the inhibition of *Candida krusei and Candida albican* and antibacterial activity was checked on *Staphylococcus aureus* and *Escherichia coli* bacteria. Neomycin and Chlorothalonil were taken as a standard for testing bacterial and fungal action, respectively. All the readings were recorded in duplicate for the ligand and the complexes in order to maintain the accuracy [45].

3. Results and discussion

3.1. Description

The conventional method of condensation was utilized to synthesis azo-dye Cu(II), Ni(II) and Co(II) chelates. Azo-dye Cu(II), Ni(II) and Co(II) complexes were obtained by refluxing method of H-BPDQ with copper/nickel/cobalt chloride salt in 2: 1 ratio (copper/nickel/cobalt: H-BPDQ) at 70 °C temperature and refluxing method. Elemental analysis data of azo-dye complexes were in good agreement with the complexes that was obtained under reflux condition. IR analysis confirms the coordination of ligand with metal ion *via* N and O atoms. Molar conductance value was very low which suggests non-electrolytic behaviour of the complexes. The antibacterial activities were evaluated against *Staphylococcus aureus* and *Escherichia coli* bacteria, and antifungal activities were checked against *Candida krusei and Candida albican* fungus at different concentrations. The biological behaviour of the complexes was more efficient in comparison to parent ligand (H-BPDQ). Furthermore, Molecular docking interactions studies were validated the complex molecule conjugation to enhance the binding and efficacy of the drug towards the target protein.

3.2. Designation of Molecular structures of ligand and its Cu(II) Ni(II) and Co(II) complexes

The designation molecular structures along with atom numbering, electron density, HOMO, LUMO and electrostatic potential of the azo-dye ligand (H-BPDQ) are shown in Fig. 1, where the same characters are presented for the metal complexes by the Fig.s 2–4. Various energetic data were calculated for the azo-dye ligand (H-BPDQ) and its Cu(II) Ni(II) and Co(II) complexes and represented in Tables 1 & 2. Molecular parameters viz; Total energy, energy of the HOMO and LUMO, energy gap, ionization energy (I), electron affinity (A), electronegativity (χ), hardness (η), softness (σ), S, inverse electronegativity (π), electrophilicity (ω) and the fraction of transferred electrons (ΔN_{max}) of the H-BPDQ and its Cu(II) Ni(II) and Co(II) complexes were screened for H-BPDQ and its Cu(II) Ni(II) and Co(II) complexes and presented in Table 3. 1.314 Å, 1.316 Å and 1.399 Å are the lengths of C(11)-N(12), N(12)-C(13) and C(18)-O(26) bonds of the ligand which were enlarged in complexes due to participation in coordination upon forming M-N(12) and M-O(26), bonds. The bond length O(26)-H(43) with the value 0.986 Å and the bond angle C(13)-O(18)- H(32) which is 107.194º disappear upon coordination as the ligand acts in a mononegative bidentate manner by losing this proton. The bond length N(7)-N(8) of H-BPDQ shows no difference as it does not contribute in complexation. These ligand's bond angles C(11)-N(12)-C(13) and C(18)-C(18)-O(26) are reduced or increased upon complexation. [42,43]. New bond angles were formed between H-BPDQ and Cu(II) Ni(II) and Co(II) ions as N(12)-M(53)-O(26), N(12)-M(53)-O(90) O(26)-M(53)-O(51), N(38)-M(53)-O(51) and N(38)-M(53)-O(52) and O(52)-M(53)-O(90) with different values ranges between (83.986º-174.697º) [42]. The previous angles are condensed or amplified on formation of complexes due to complication. The stability of these complexes follow the Irving Williams order according to E_{Gap} data as the Cu(II) Ni(II) and Co(II). The lower HOMO vitality esteems demonstrate that molecules giving electron capacity is the weaker. On opposite, the higher HOMO vitality suggests that the molecule is a decent electron giver [42]. LUMO vitality shows the capacity of an atom getting electron. Further, in this study the stability of the ligand and its complexes were also evaluated from the molecular orbital structures from which the quantum chemical parameters were calculated using the HOMO and LUMO energies [42]. The vitality of association of a point positive charge (an electrophile) with the electrons and the core of a molecule is called electrostatic potential. Negative electrostatic possibilities demonstrate zones that are inclined to electrophilic assault [43,44]. The computed reactivity parameters shown in Table 3 reveals that the The calculated η, σ, χ, π, ω and ε parameters support that the Cu(II) complex inhibitor has the most effective corrosion inhibition effect. The lower χ value of the inhibitor shows that the iron metal will form a bond by taking electrons from the inhibitor compound and the higher ΔN value of the inhibitor shows that it will be

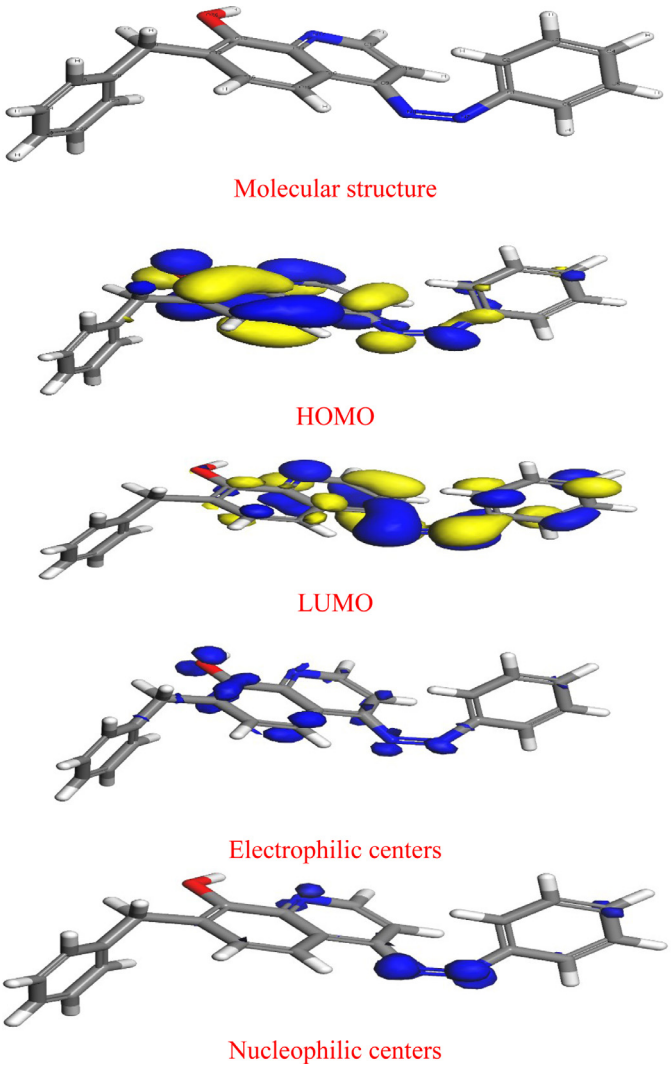

Fig. 1. The molecular structure, HOMO, LUMO, Electrophilic centers and Nucleophilic centers of the ligand.

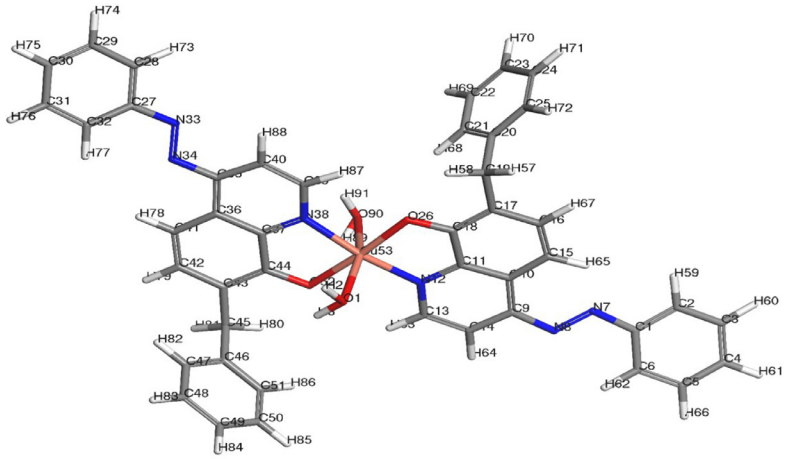

Molecular structure

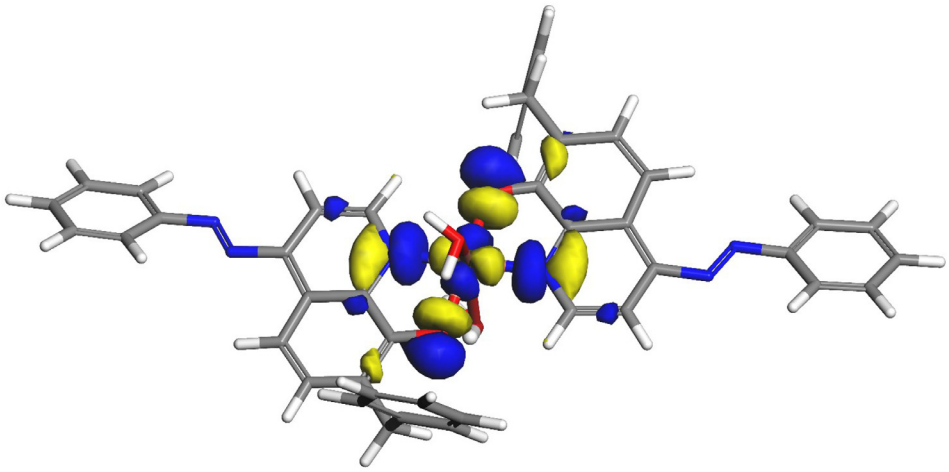

HOMO

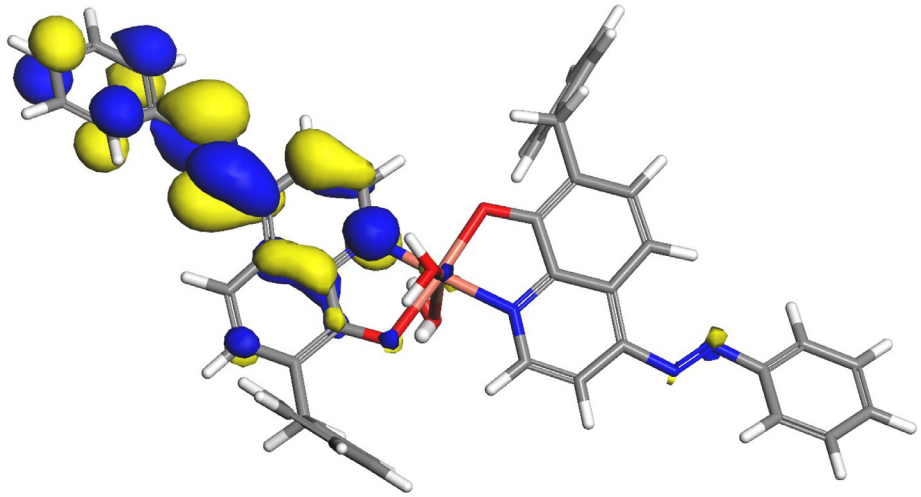

LUMO

Fig. 2. The molecular structure, HOMO, LUMO and electrostatic potential of Cu^{II}-L complex.

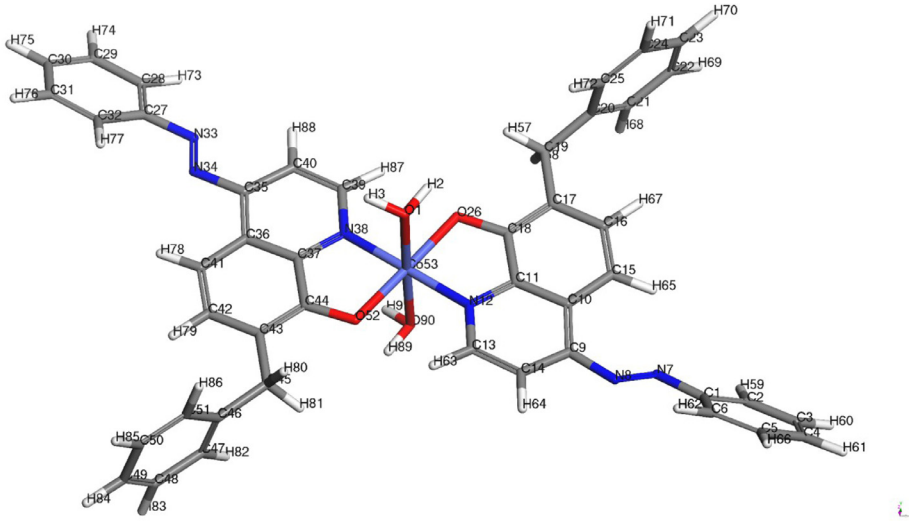

Molecular structure

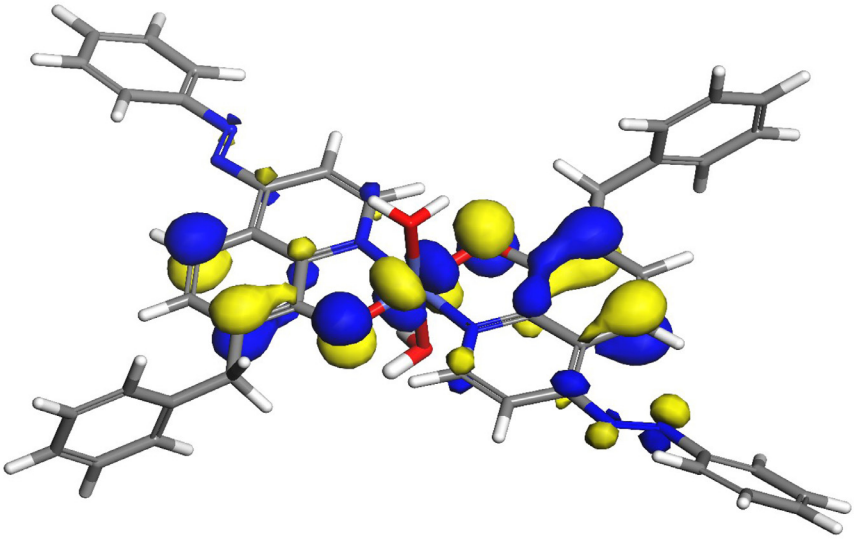

HOMO

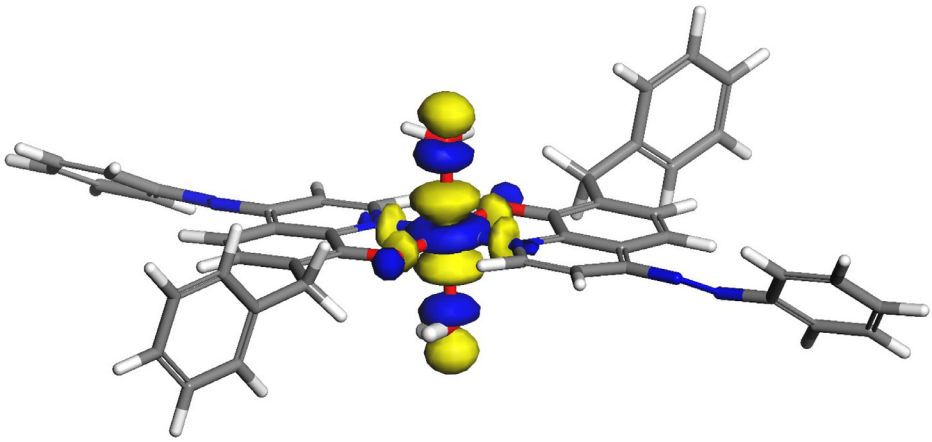

LUMO

Fig. 3. The molecular structure, HOMO, LUMO and electrostatic potential of Co^{II}-L complex.

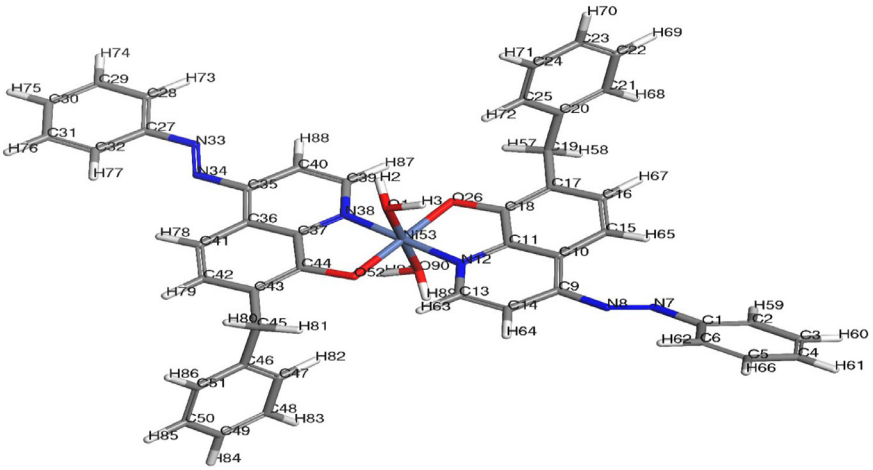

Molecular structure

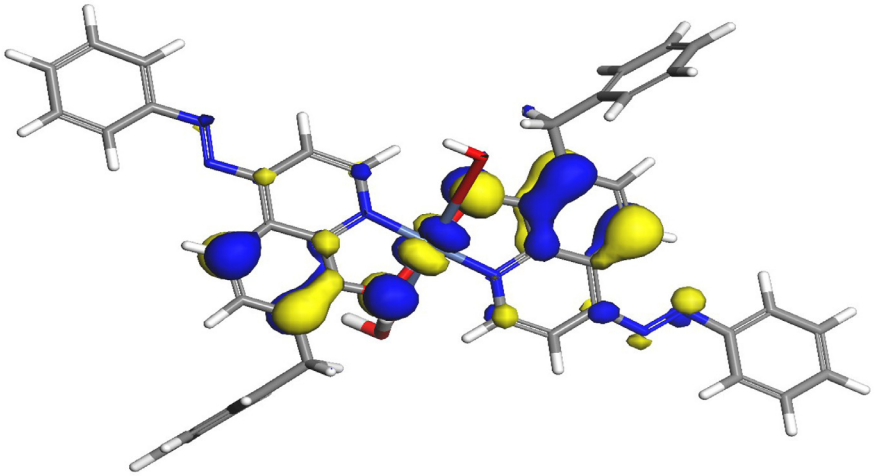

HOMO

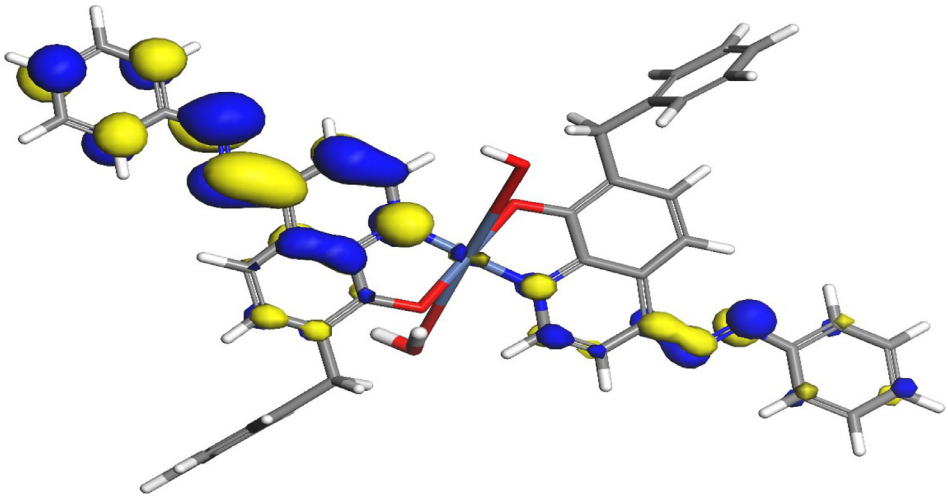

LUMO

Fig. 4. The molecular structure, HOMO, LUMO and electrostatic potential of Ni^{II}-L complex.

Table 1
Comparison between the bond lengths of H-BPDQ and its Cu(II), Ni(II) and Co(II) complexes.

Bond length	H-BPDQ	Cu^{II} - BPDQ	Ni^{II} - BPDQ	Co^{II} - BPDQ
C(1)-N(7)	1.402	1.406	1.399	1.402
N(7)-N(8)	1.388	1.389	1.388	1.389
C(11)-N(12)	1.314	1.336	1.342	1.298
C(18)-O(26)	1.399	1.382	1.413	1.381
O(26)-H(43)	0.986	–	–	–
C(27)-N(33)	–	1.410	1.395	1.406
N(33)-N(34)	–	1.387	1.388	1.389
C(37)-N(38)	–	1.341	1.389	1.389
C(44)-O(52)	–	1.398	1.400	1.399
N(12)-M(53)	–	1.412	1.411	1.410
O(26)-M(53)	–	1.411	1.412	1.410
N(38)-M(53)	–	1.334	1.366	1.343
O(51)-M(53)	–	1.302	1.303	1.304
O(52)-M(53)		1.998	1.996	1.997
O(90)-M(53)	–	1976	1.968	1.970

Table 2
Comparison between the bond angles of H-BPDQ and its Cu(II), Ni(II) and Co(II) complexes.

Bond angle	H-BPDQ	Cu^{II} - BPDQ	Ni^{II} - BPDQ	Co^{II} - BPDQ
C(1)-N(7)-N(8)	123.856	117.332	117.817	119.043
N(7)-N(8)-C(9)	121.258	121.264	121.317	120.349
C(11)-N(12)-C(13)	118.084	119.636	119.958	120.343
C(218)-O(26)-H(43)	107.194	–	–	–
C(27)-N(33)-N(34)	–	105.368	105.371	105.374
N(33)-N(34)-C(35)	–	104.352	104.685	103.941
C(37)-N(38)-C(39)	–	117.897	118.003	118.020
N(12)-M(53)-O(26)	–	89.713	83.986	85.534
N(12)-M(53)-O(90)	–	93.369	94.047	93.322
O(26)-M(53)-O(51)	–	92.787	93.082	94.563
N(38)-M(53)-O(51)	–	88.253	91.804	93.896
N(38)-M(53)-O(52)		173.568	174.697	169.734
O(52)-M(53)-O(90)		90.147	88.804	89.342

Table 3
E_T, E_{HOMO} and E_{LUMO}, E_g, I, A, χ, η, σ, S, π, ω and ΔN_{max} of H-BPDQ and its Cu(II), Ni(II) and Co(II) complexes.

Parameter	H-BPDQ	Cu^{II} - BPDQ	Ni^{II} - BPDQ	Co^{II} - BPDQ
E_T, a.u.	-2415.58	-2864.44	-2988.16	-2904.89
E_{HOMO}, a.u.	-0.23357	-0.23014	-0.22752	-21576
E_{LUMO}, a.u.	-0.11475	-0.14578	-0.15482	-0.17668
E_g, eV	3.1576	2.9878	2.6635	0.4852
I, eV	6.24575	5.89374	4.8524	4.70634
A, eV	3.02546	3.55452	3.4712	3.05284
χ, eV	4.98645	5.03574	4.85642	5.17784
η, eV	1.87696	1.45889	1.28696	0.37576
Σ	0.79414	0.86899	0.82422	4.36384
S, eV	0.38868	0.48883	0.59008	14.5283
π,eV	-3.8563	-5.4567	-4.88228	-5.6073
ω, eV	8.63524	10.41264	10.69876	46.12897
ΔN_{max}	2.69355	4.58472	5.86943	18.6393

better adsorbed to the metal surface and the corrosion inhibition effect will increase [43]. Atomic charges of the H-BPDQ ligand and its Cu(II) Ni(II) and Co(II) complexes calculated by the Mullikan method [46] are given in Tables 4 and 5. As can be seen, higher charge density was found at C18 than for the other ring carbon atoms on the ligand. On the other hand, C18, which is connected to oxygen atom (O26), has the maximum charge -0.704).

3.3. NMR spectra of H-BPDQ

The ^{1}H NMR of the obtained **H-BPDQ** showed the characteristic NMR signals and the data is shown in Fig. 5. The ^{1}H NMR spectrum (Fig. 5) of ligand (H-BPDQ) shows a singlet at δ 11.34 ppm (s, 1H, OH) due to the proton of hydroxyl group, another sin-

Table 4
The Mulliken atomic charges of H-BPDQ ligand.

Atom	Charge	Atom	Charge
C (1)	0.234	C (23)	-0.140
C (2)	-0.199	C (24)	-0.150
C (3)	-0.137	C (25)	-0.138
C (4)	-0.142	O (26)	-0.704
C (5)	-0.139	H (27)	-0.167
C (6)	-0.178	H (28)	0.163
N (7)	-0.193	H (29)	0.146
N (8)	-0.202	H (30)	0.144
C (9)	0.199	H (31)	0.144
C (10)	0.073	H (32)	0.159
C (11)	0.189	H (33)	0.142
N (12)	-0.430	H (34)	0.160
C (13)	-0.016	H (35)	0.165
C (14)	-0.241	H (36)	0.151
C (15)	-0.238	H (37)	0.207
C (16)	-0.173	H (38)	0.167
C (17)	0.031	H (39)	0.148
C (18)	0.366	H (40)	0.137
C (19)	-0.438	H (41)	0.135
C (20)	0.157	H (42)	0.134
C (21)	-0.176	H (43)	0.133
C (22)	-0.172		

Table 5
The Mulliken atomic charges of Cu(II), Ni(II) and Co(II) complexes (1-3), respectively.

Atom	Charge			Atom	Charge		
	1	2	3		1	2	3
C (1)	0.181	0.183	0.188	C (47)	-0.251	-0.253	-0.253
C (2)	-0.222	-0.221	-0.225	C (48)	-0.209	-0.213	-0.207
C (3)	-0.207	-0.211	-0.211	C (49)	-0.217	-0.219	-0.216
C (4)	-0.205	-0.208	-0.206	C (50)	-0.209	-0.213	-0.207
C (5)	-0.204	-0.207	-0.203	C (51)	-0.249	-0.252	-0.250
C (6)	-0.244	-0.242	-0.247	O (52)	-0.570	-0.573	-0.572
N (7)	-0.194	-0.198	-0.194	M (53)	0.534	0.536	0.538
N (8)	-0.189	-0.192	-0.183	O (54)	-0.809	-0.812	-0.814
C (9)	0.164	0.166	0.167	H (55)	0.428	0.427	0.425
C (10)	0.028	0.029	0.031	H (56)	0.451	0.448	0.457
C (11)	0.177	0.179	0.176	H (57)	0.226	0.229	0.224
N (12)	-0.332	-0.333	-0.337	H (58)	0.269	0.271	0.263
C (13)	-0.093	-0.095	-0.096	H (59)	0.230	0.232	0.237
C (14)	-0.252	-0.254	-0.257	H (60)	0.211	0.209	0.204
C (15)	-0.289	-0.287	-0.292	H (61)	0.211	0.209	0.204
C (16)	-0.241	-0.240	-0.243	H (62)	0.237	0.238	0.232
C (17)	0.056	0.058	0.053	H (63)	0.251	0.253	0.253
C (18)	0.338	0.336	0.334	H (64)	0.230	0.233	0.237
C (19)	-0.620	-0.622	-0.623	H (65)	0.251	0.248	0.253
C (20)	0.158	0.156	0.157	H (66)	0.211	0.208	0.204
C (21)	-0.250	-0.253	-0.255	H (67)	0.207	0.203	0.201
C (22)	-0.205	-0.211	-0.208	H (68)	0.244	0.252	0.251
C (23)	-0.217	-0.219	-0.216	H (69)	0.204	0.205	0.207
C (24)	-0.207	-0.209	-0.208	H (70)	0.198	0.203	0.199
C (25)	-0.257	-0.259	-0.256	H (71)	0.198	0.203	0.199
O (26)	-0.540	-0.542	-0.546	H (72)	0.195	0.202	0.189
C (27)	0.173	0.175	0.177	H (73)	0.224	0.228	0.227
C (28)	-0.220	-0.225	-0.226	H (74)	0.213	0.219	0.218
C (29)	-0.220	-0.225	-0.226	H (75)	0.212	0.220	0.216
C (30)	-0.207	-0.209	-0.202	H (76)	0.212	0.20	0.215
C (31)	-0.203	-0.205	-0.208	H (77)	0.243	0.246	0.249
C (32)	-0.243	-0.245	-0.246	H (78))	0.230	0.234	0.233
N (33)	-0.173	-0.174	-0.177	H (79)	0.206	0.203	0.208
N (34)	-0.193	-0.196	-0.201	H (80)	0.247	0.248	0.249
C (35)	0.161	0.163	0.165	H (81)	0.236	0.232	0.234
C (36)	0.054	0.056	0.057	H (82)	0.216	0.218	0.215
C (37)	0.154	0.157	0.157	H (83)	0.201	0.206	0.208
N (38)	-0.357	-0.359	-0.356	H (84)	0.201	0.206	0.208
C (39)	-0.109	-0.111	-0.113	H (85)	0.202	0.207	0.209
C (40)	-0.285	-0.287	-0.289	H (86)	0.207	0.212	0.208
C (41)	-0.300	-0.303	-0.308	H (87)	0.278	0.279	0.274
C (42)	-0.254	-0.255	-0.256	H (88)	0.241	0.244	0.247
C (43)	0.058	0.059	0.062	H (89)	0.445	0.447	0.449
C (44)	0.302	0.304	0.305	O (90)	-0.847	-0.844	-0.849
C (45)	0.609	0.611	0.611	H (91)	0.416	0.414	0.418
C (46)	0.168	0.169	0.171				

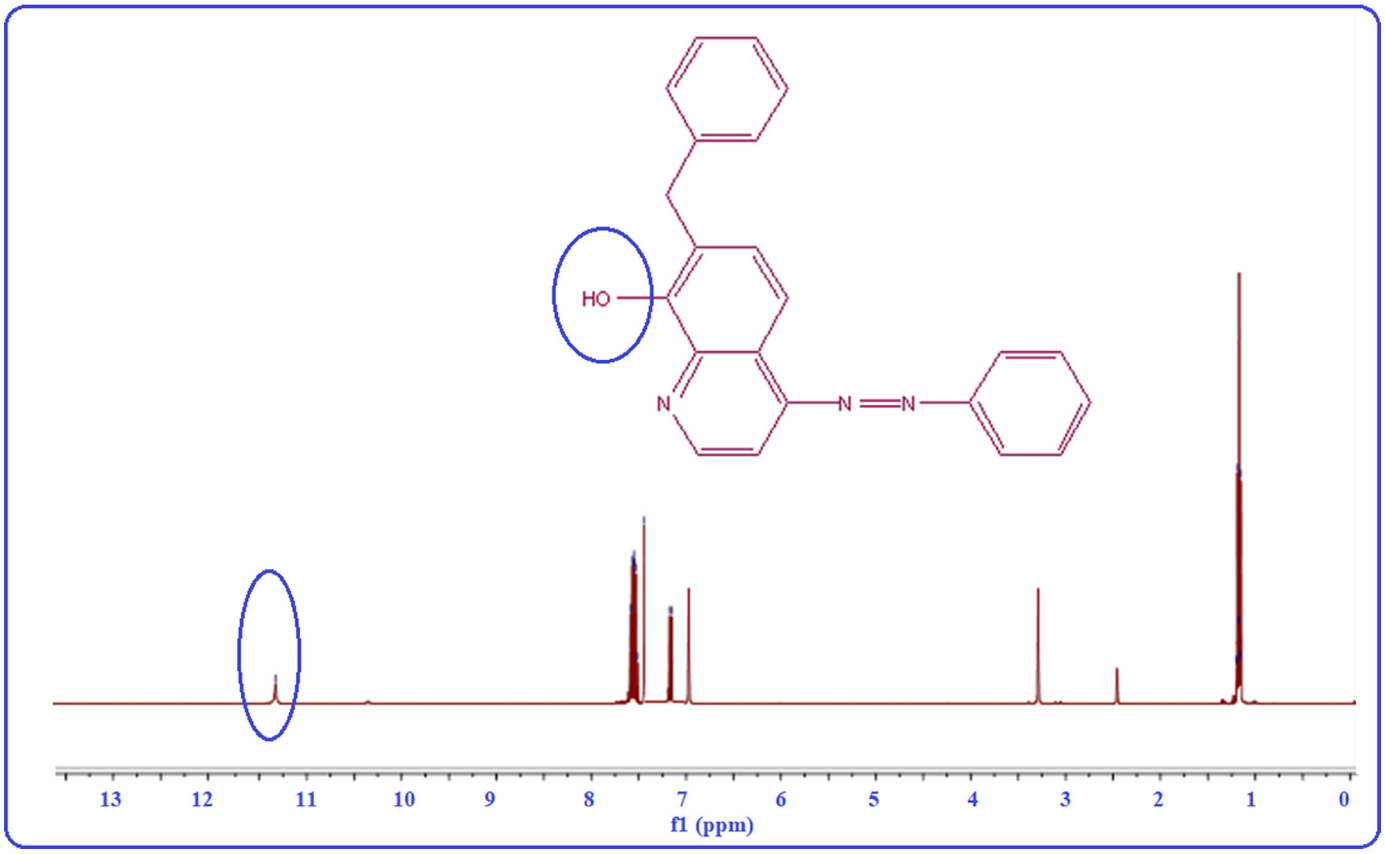

Fig. 5. ^{1}H NMR spectrum of **H-BPDQ**.

glet at δ 3.37 ppm (s, 2H, $2CH_2$) due to protons of one methylene groups and a multiplet at δ 6.82–7.63 ppm due to the presence of one hetero and three aromatic rings in the H-BPDQ. The ^{13}C NMR (Fig. 6) spectrum of **H-BPDQ** showed signals at δ 42, 62–133, 142, 148 and 168 ppm, indicating the presence of CH_2, phenyl, C=N and C–OH carbon, respectively. The ^{15}N NMR spectrum of **H-BPDQ** (Fig. 7) was also obtained. Signals of the N(azo-dye) and N (quinoline) were appeared at centered at 132 and 176 ppm, respectively.

3.4. Infrared spectroscopy

The IR spectra provide valuable information regarding the nature of the functional group attached to the metal atom. The IR spectral results of Schiff bases and their metal chelates are showed in Fig. 8, which indicates that **H-BPDQ** is coordinated to metal atom in two ways, thus ligand acting in bidentate manner. The IR spectra of free ligand was compared with those of the complexes in order to confirm the coordination of azo-dye compound. The IR spectra of the free **H-BPDQ** ligand shows a strong band in the region 1618 cm^{-1} that is characteristic of the (–N=C–)quinoline ring [47-49]. Coordination of the (–N=C–)quinoline to the metal through the nitrogen atom is expected to reduce the electron density in the (–N=C–)quinoline frequency. The band due to quinoline nitrogen ν(C=N) shows a modest decrease in the stretching frequency for the complexes and is shifted to lower frequencies, appearing around 1688–1578 cm^{-1}, which indicates the involvement of (–N=C–)quinoline nitrogen in coordination to the metal ions [47-49]. The νC–O band appeared at 1243 cm^{-1}, respectively, are shifted toward lower sides in the Cu(II), Ni(II) and Co(II) complexes indicating coordination's via C–O [48,49]. Whereas, the –OH stretching vibration band was noted at 3055 cm^{-1} [48,49] and this band is absent after chelation with copper ion [50,51]. In the spectra of metal(II) chelates the bands from M-O and M-N stretching vibrations appear at about 579-594 and 444-452 cm^{-1}[52]. The complexes (1–3) also display bands due to coordinated/ hydrated water molecules [51]. The bands in the range 745–845 cm^{-1} and 612–632 cm^{-1} appeared in the spectra of these complexes which may be assigned to ρr(H_2O) and ρw(H_2O) [48-52]. The bands at 1522-1529 and 1376–1378 cm^{-1} in all the complexes are due to the ν(N=N) and ν(CH_2) frequencies, respectively, were not affected upon complexation. Furthermore, the azo-dye and aliphatic protons are not greatly affected upon complexation.

3.5. Mass spectra

Electron impact mass spectra (EIMS) of the H-BPDQ and complex (1) (Fig. 9a and b) confirm the proposed formula by showing the following peaks:

Ligand H-BPDQ: Appearance of final peak at 339.3 amu ($C_{22}H_{17}N_3O$ calculated atomic mass 143amu) and other peaks at 231.2, 163.3, 109.9, and 106.2 amu may be due to different fragments. The intensity of these peaks gives an idea of the stability of these fragments.

Complex (1): Under the Electron impact mass spectral (EIMS) study it gives a final peak at 812.3 amu confirms the proposed formula ($C_{44}H_{40}CuN_6O_6$ calculated atomic mass 159amu) and other peaks at 132.2, 228.8, 231.3, 362.1, 374.1, 375.2, 703.3 and 725.5 amu may be attributed to different fragments.

3.6. Molar conductance

The molar conductance of Cu(II), Ni(II) and Co(II) complexes (exists in the region 5.21-6.85 $\Omega^{-1}cm^2mol^{-1}$ using DMSO as sol-

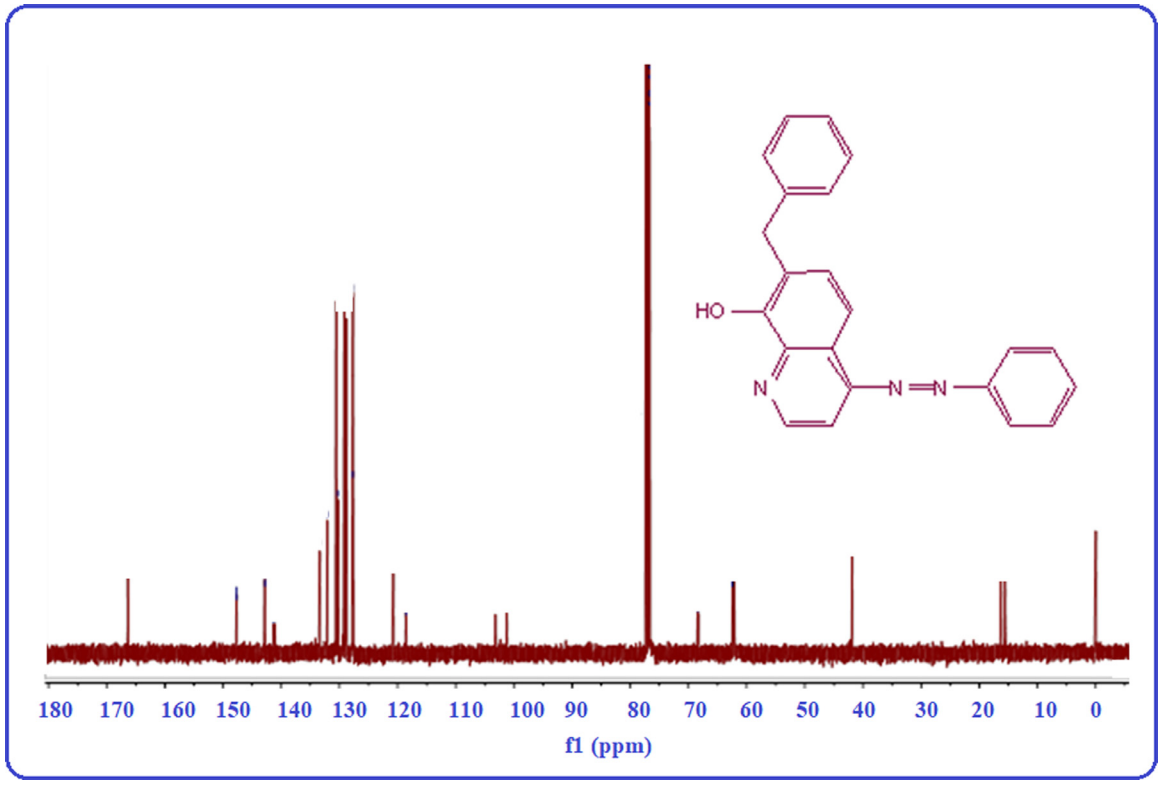

Fig. 6. ^{13}C NMR spectrum of **H-BPDQ**.

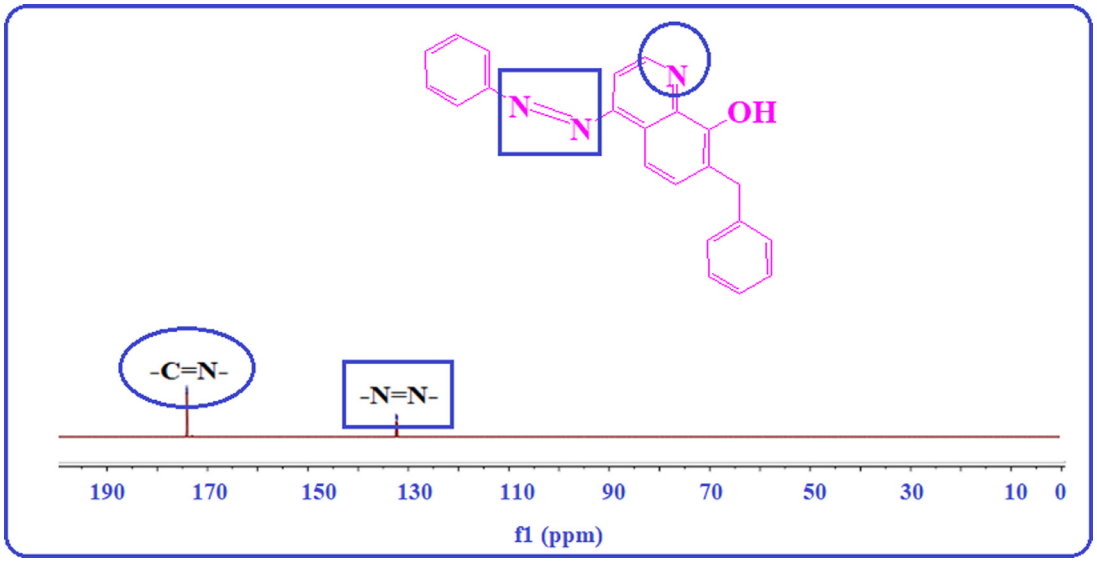

Fig. 7. ^{15}N NMR spectrum of **H-BPDQ**.

vent. The value of molar conductance concludes the participation of anions in the complexation and confirms the non-electrolyte nature of complexes [53].

3.7. Magnetic moment

Cu(II), Ni(II) and Co(II) complexes under analysis, illustrate magnetic moment at 1.83, **2.8**2 and **3.8**8 B.M. at room temperature, which corresponds to the single, two and three unpaired electrons, respectively. According to the data, the paramagnetic behaviour was considered for all the synthesized complexes **(1-3)** and proposed to have octahedral geometry [53].

3.8. Electronic Spectra

The electronic spectrum of **H-BPDQ** (Fig. 10a) showed six bands in the UV region at 42,918, 36,496, 34,246, 29,585, 24,271 and

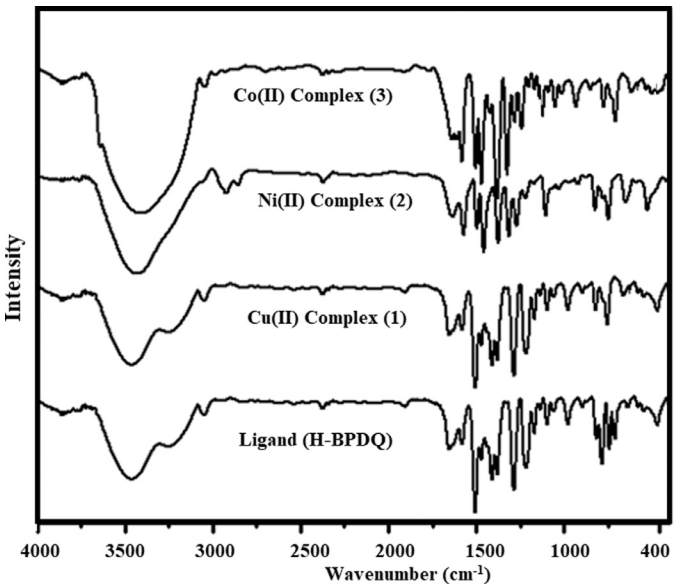

Fig. 8. IR spectra of **H-BPDQ** ligand and its complexes **(1-3).**

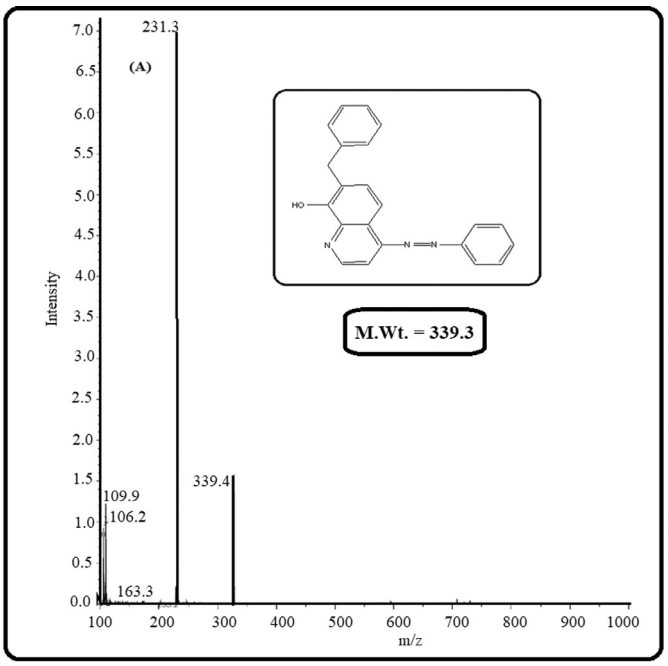

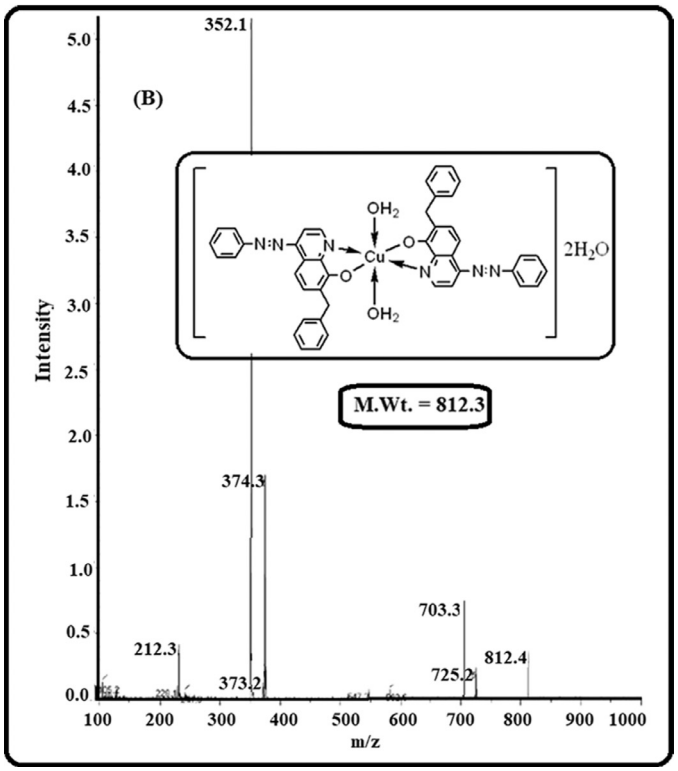

Fig. 9. Mass spectra of (a) H-BPDQ and (b) Cu(II) complex 1.

23,148 cm^{-1} were assigned to π–π^* and n–π^* transitions of azomethine groups.

The DMSO solution was used to record the electronic spectra of Cu(II), Ni(II) and Co(II) complexes. In the Cu(II) complex (Fig. 10b), the absorption bands exist in the range 12115cm^{-1} (ε = 30 $Lmol^{-1}$ cm^{-1}), 18633cm^{-1} (ε = 38 $Lmol^{-1}$ cm^{-1}) and 24474-26046 cm^{-1} (ε = 44–51 $Lmol^{-1}$ cm^{-1}). These absorption bands suggest $^2B_{1g}\rightarrow{}^2A_{1g}$ ($d_x{}^2{}_{-y}{}^2\leftarrow d_z{}^2$), $^2B1g\rightarrow{}^2B_{2g}$ ($d_x{}^2{}_{-y}{}^2\leftarrow d_{xy}$) and $^2B_{1g}\rightarrow{}^2E_g$($d_x{}^2{}_{-y}{}^2\leftarrow d_{xz}$, d_{yz}) transitions, respectively. An additional band in spectra appeared in the scale of 33999cm^{-1} (ε = 65 $Lmol^{-1}$ cm^{-1}), which is known as a charge transfer band. The elongated hexagonal environment was recommended around the Cu(II) ion [53].

For Ni(II) complex (Fig. 10c), different absorption bands found in the range 10682cm^{-1} (ε = 27 $Lmol^{-1}$ cm^{-1}), 15236cm^{-1} (ε = 32 $Lmol^{-1}$ cm^{-1}), 24110cm^{-1} (ε = 43 $Lmol^{-1}$ cm^{-1}) and 34654 cm^{-1} (ε = 74 $Lmol^{-1}$ cm^{-1}). These bands attributed to $^3A_{2g}\rightarrow{}^3T_{2g}$, $^3A_{2g}\rightarrow{}^3T_{1g}$, $^3A_{2g}\rightarrow{}^3T_{1g}$ transitions, respectively. The absorption band at 34654 cm^{-1} (ε = 118 $Lmol^{-1}$ cm^{-1}) is due to the charge transfer. Octahedral geometry was revealed by above transitions for Ni(II) complexes [53]. In the Co(II) complex (Fig. 10d), the absorption bands exist in the range 13458cm^{-1}(ε = 13 $Lmol^{-1}$ cm^{-1}), 19967 cm^{-1} (ε = 39 $Lmol^{-1}$ cm^{-1}) and 28926 cm^{-1} (ε = 56 $Lmol^{-1}$ cm^{-1}). These absorption bands suggest $^2A_{1g}\rightarrow{}^2B_{1g}$, $^2T_1g\rightarrow{}^2T_{2g}$ and $^2T_{1g}\rightarrow{}^2E_g$ transitions, respectively. An additional band in spectra appeared in the scale of 34568 cm^{-1} (ε = 112 $Lmol^{-1}$ cm^{-1}), which is known as a charge transfer band. The elongated hexagonal environment was recommended around the Cu(II) ion [53].

3.9. Ligand field parameters

The different ligand field parameters such as Racah interelectronic parameter (B), ligand field splitting (Dq), the nephelauxetic parameter (β) were calculated for Ni(II) complexes. The ligand field stabilization energy (LFSE) for different Ni(II) and Co(II) complexes was also calculated [54]. The nephelauxetic parameter β is calculated by using the relation: β = B (complex) / B (free ion). To calculate the nephelauxetic parameter (β), the value of $B_{free\ ion}$ for Ni(II) and Co(II) ions are 1041 and 1047cm^{-1}, respectively. The values of β for the Ni(II) and Co(II) complexes under investigation are 0.36 and 0.46, respectively, which indicates that the covalent character of complexes is high [55]. The values Dq, B and LFSE) are at (1152 and 1142), (377 and 478) and (163 and 158), respectively.

3.10. The EPR spectra

The EPR spectrum (Fig. 11) of the Cu(II) complex **(1)** as polycrystalline sample was characterized at room temperature (RT).

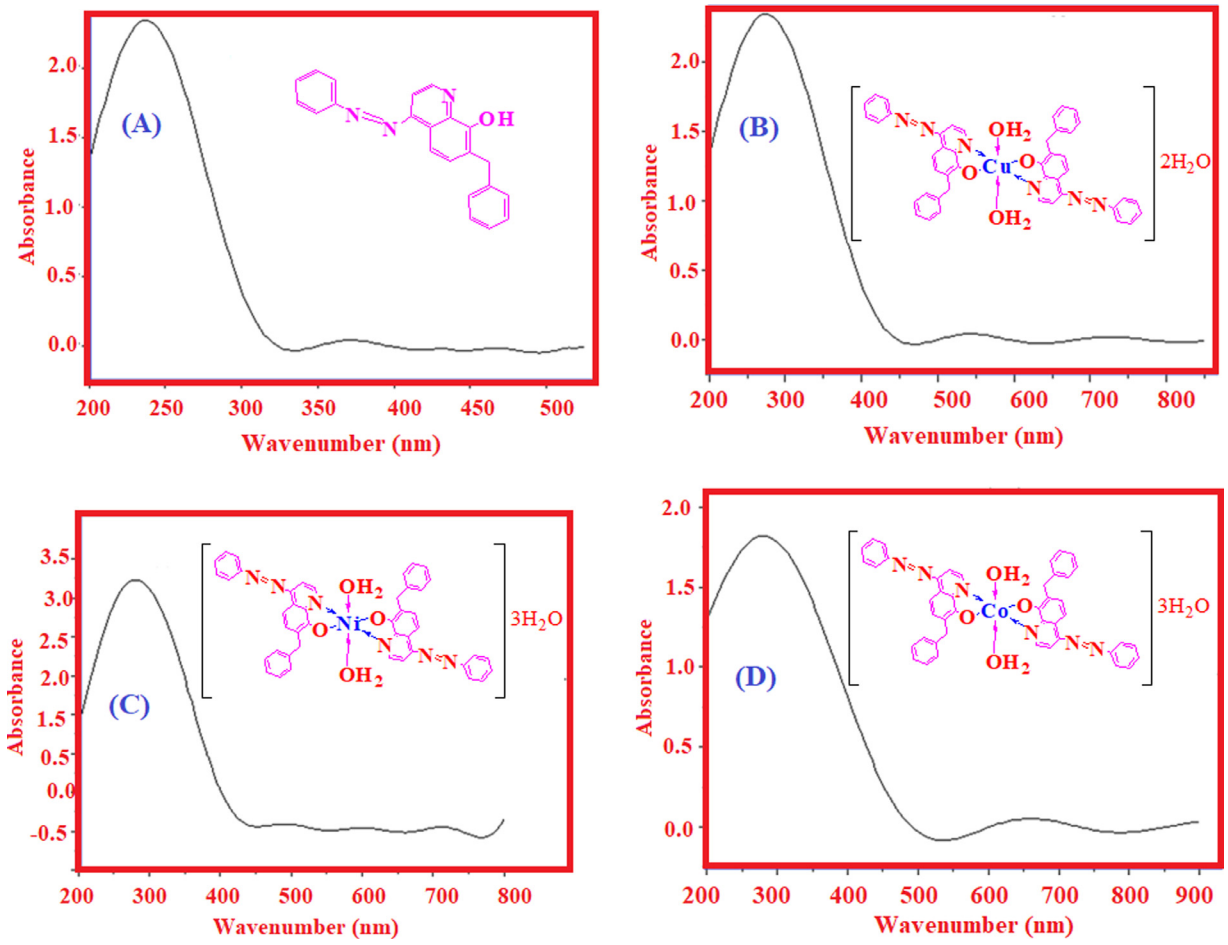

Fig. 10. Electronic spectra of (a) H-BPDQ and (b) Cu(II) complex, (c) Ni(II) complex and (d) Co(II) complex.

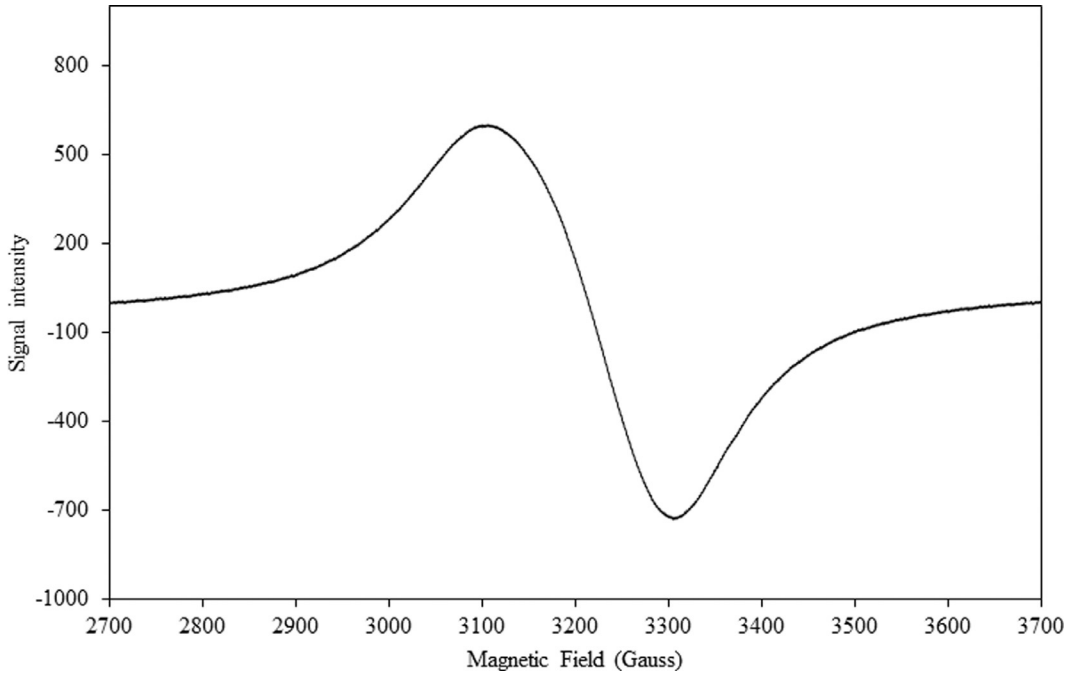

Fig. 11. EPR spectra of Cu(II) complex **1**.

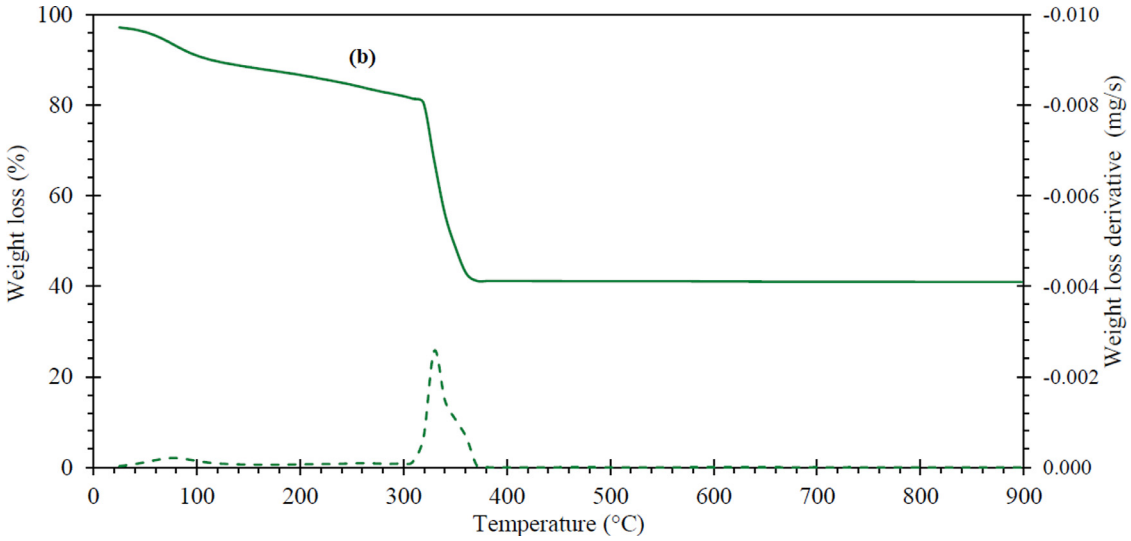

Fig. 12. TG–DTG curves of (a) Cu complex **(1)** and (b) Ni complex **(2)**.

The following expressions were used to calculate g_{iso} and geometric parameter (G) values:

$$giso = \frac{g_{||} + 2g_{\perp}}{3}$$

and

$$G = \frac{g_{||} - 2.0023}{g_{\perp} - 2.0023}$$

The exchange interaction between the copper centers was predicted by the geometric parameter G. If G < 4, it suggests significant interaction in solid complexes but if G > 4 suggests negligible exchange interaction [56,57]. The evaluated values of *g* tensor parameters i.e., $\mathbf{g}_{||}$= 2.23 and $\mathbf{g}_{\perp}$ = 2.12 for the complex, follow the trend $\mathbf{g}_{||} > \mathbf{g}_{\perp} > 2.0023$, which confirm that the unpaired electron is in $d_x^2-_y^2$ ground state orbital [56,57]. Thus, it is confirmed to possess tetragonal elongated geometry with D_{4h} symmetry. The complexes under investigation possessed G value at 2.99. Parameters of the orthorhombic g molecule are perceived for the geometries of octahedral with the coordination number of six [58].

3.11. The thermal decompositions

The thermal decomposition of complex **1** (Fig. 12a) showed 1st stage at 22-94°C with a mass loss of 8.14 % (cal. 8.22 %) due to removal of two hydrated H_2O molecules. The 2nd step occurred at 94-308°C with loss of 32.74 % of the total weight (cal.32.81 %) assignable to elimination of two coordinated water molecules, and partial decomposition of the organic ligand. The last step at 308-900°C with removal of 41.27 % the total weight (cal. 41.39 %) corresponded to further decomposition of the organic ligand with production of CuO as final product.

For complex **2** (Fig. 12b) the 1st step appeared at 22-96°C with mass loss 10.78 % (calc. 10.60 %) is due to removal of three hydrated H_2O molecules. The 2nd step started at 100°C to 305°C and correspond to removal of two coordinated H_2O molecules, and partial degradation of the organic ligand with mass loss of 33.16 % (calc. 33.30 %). The 3rd stage occurred within 305-900°C with mass loss of 30.63 % (calc. 30.87 %) and assigned to further decomposition of the organic moiety leading to the formation of NiO as ultimate product.

Also, the decomposition kinetics were calculated for the Cu(II) and Ni(II) complexes (**1** and **2**) (Table S1; Fig. S1). The kinetic parameters (E, A, ΔH, ΔS and ΔG) were calculated using two methods, Coats–Redfern (CR) [59], Horowitz–Metzger (HM) [60] and Piloyan–Novikova (PN) [61]. The value of ΔG increases significantly for two complexes [62,63]. The ΔS values are positive in some steps indicating a dissociation character of degradation or a consequence of the entropy changes in-between the gaseous and solid products (formation of a new crystalline lattice), but the negative ΔS values suggest the decomposition via abnormal pathway [64]. The positive ΔH values mean that the decomposition processes are endothermic. The high E values of the complexes reflect the thermal rigidity of them.

Table 6
Biological activity data of synthesized compounds.

Compd no.	Concentration (ppm)	Fungal Inhibition (mm)		Bacterial Inhibition (mm)	
		C.albicans	*C.krusei*	*S.aureus*	*E.coli*
H-BPDQ	1000	15.8	19.7	13.4	15.8
	750	8.6	13.8	10.3	12.7
	500	6.3	11.8	8.3	11.3
	250	NA	5.3	5.5	9.4
Complex 1	1000	17.9	19.1	12.7	16.5
	750	16.2	12.8	9.6	13.8
	500	9.3	11.0	9.3	11.7
	250	5.6	10.1	6.5	8.2
Complex 2	1000	18.9	19.7	13.2	17.7
	750	16.7	18.2	12.3	16.3
	500	10.7	16.8	10.4	15.4
	250	6.6	12.5	9.6	10.7
Complex 3	1000	23.5	20.9	15.3	19.3
	750	20.6	19.9	12.4	18.7
	500	18.5	19.2	11.9	17.8
	250	17.8	18.7	10.4	16.7
Standard drug	1000	22.4	22.6	21.4	22.4
	750	21.2	21.5	20.5	21.6
	500	20.5	21.0	20.2	20.3
	250	19.5	20.1	19.8	19.2

3.12. Antimicrobial action

The antimicrobial evaluation of the H-BPDQ ligand and its metal (II) chelates (1-3) were conducted by using Well diffusion method. The antibacterial activities were evaluated against *S.aureus* and *E.coli* bacteria, whereas antifungal activities were checked against *C.albicans* and *C.krusei* fungus at different concentrations. The medium used to screen the antibacterial and antifungal activity is Sabround Dextrose Agar and Nutrient agar respectively.

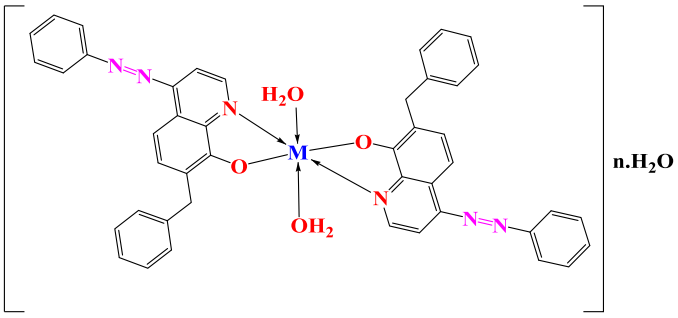

M = Cu(II); n = 2, Ni(II); n = 3 and Co(II); n =3

Fig. 13. Schematic representation of the Cu(II), Ni(II) and Co(II) complexes.

The fungal growth inhibition was expressed in mm. Chlorothalonil and Neomycin were employed as standard drugs for examining antibacterial and antifungal activities, respectively. The biocide activities of all the compounds were confirmed by the antimicrobial screening data. On comparing ligand with its metal (II) chelates **(1-3)**, it was found that complexes possess better inhibition character. The enhancement of antimicrobial activities in ligand after complex formation is based on Overtone's concept and chelating theory [65]. Lipophilicity of the metal (II) chelates **(1-3)** increases as the metal ion charge decreases, which breaks the permeability obstruction of the cell and retards the processes of the cell [66]. The biological screening demonstrates more inhibition as the concentration increases (Table 6) [67].

4. Conclusions

Synthesis, spectroscopic and thermal studies were carried out for 7-benzyl-4-(phenyldiazenyl) quinolin-8-ol (HBPDQ) complexes with divalent copper, nickel and cobalt ions. These complexes were characterized by IR, UV-vis, NMR (^{1}H, ^{13}C and ^{15}N), mass spectrometry and elemental analysis, along with molar conductivity, magnetic susceptibility measurements and thermal analysis. The synthetic procedures results are 1:2 (metal: ligand) in favor of bidentate chelate with deprotonated hydroxyl oxygen (-OH) group and adjacent quinoline nitrogen and in favor of six-coordinate Oh rearrangements centered by Co(II), Ni(II) and Cu(II) ions. DFT calculations are found in good agreement with experimental data where the overall trend of metal complexes stability is in the order Cu > Ni > Co. (Fig. 13). The antifungal and antibacterial investigation proves the enhancement of antimicrobial activities of azo-dye M(II) chelates as compared to the parent ligand.

Credit author statement

A.A., M.D. and R.A. played an important role in the project design and execution, while M.D. and R.A. carried out the experimental work. A.A. and R.A. played a crucial role in the characterization and elucidation of the results. M.D. carry out the quantum chemical calculation. All authors shared a part in compiled the data and prepared the manuscript. All authors read and approved the final manuscript.

Declaration of Competing Interest

We wish to confirm that there are no known conflicts of interest associated with this publication and there has been no significant financial support for this work that could have influenced its outcome. We confirm that the manuscript has been read and approved by all named authors and that there are no other persons who satisfied the criteria for authorship but are not listed. We further confirm that the order of authors listed in the manuscript has been approved by all of us. We confirm that we have given due consideration to the protection of intellectual property associated with this work and that there are no impediments to publication, including the timing of publication, with respect to intellectual property. We confirm that we have provided a current, correct email address which is accessible by the Corresponding Author..

Acknowledgments

This research project was supported by a grant from the "Research Center of the Female Scientific and Medical colleges", Deanship of Scientific Research, King Saud University.

Supplementary materials

Supplementary material associated with this article can be found, in the online version, at doi:10.1016/j.molstruc.2020.128984.

References

[1] H.I. Ugras, I. Basaran, T. Kilic, U. Cakir, Synthesis, complexation and antifungal, antibacterial activity studies of a new macrocyclic schiff base, J. Heterocyclic Chem. 43 (2006) 1679–1684.
[2] F.M. Morad, M.M.EL. Ajaily, S.B. Gweirif, Preparation, physical characterization and antibacterial activity of Ni (II) schiff base complex, J. Sci. Appl. 1 (2007) 72–78.
[3] E.A Elzahany, K.H. Hegab, S.H. Khalil, K.N.S. Youssef, Synthesis, characterization and biological activity of some transition metal complexes with schiff bases derived from 2-formylindole, salicylaldehyde, and n-amino rhodanine, Austr. J. Basic Appl. Sci. 2 (2) (2008) 210–220.
[4] G.K. Rao, K.N. Venugopala, P.N. Sanjay pai, Novel Schiff Bases of 4-Hydroxy 6-Carboxhydrazino Benzofuran Analogs: Synthesis and Pharmacological Study, J. Pharm. Toxi. 2 (5) (2007) 481–488.
[5] S. Bairagi, A. Bhosale, M.N. Deodhar, Design, Synthesis and Evaluation of Schiff's Bases of 4-Chloro-3-coumarin aldehyde as Antimicrobial Agents, E-J. Chem. 6 (3) (2009) 759–762.
[6] Y.I. Yi, X.Q. Wei, M.G. Xie, Z.Y. Lu, Synthesis and color-tunable fluorescence properties of Schiff base zinc (II) complexes used as electroluminescent materials, Chin. Chem. Lett. 15 (2004) 525–528.
[7] M.V. Aanandhi, S. George, V. Vaidhyalingam, Synthesis and antimicrobial activities of 1-(5-substituted-2-oxo indolin-3-ylidene)-4-(substituted pyridin-2-yl)thiosemicarbazide, ARKIVOC (xi) (2008) 187–194.
[8] M.d.S. Hossain, C.M. Zakaria, M.M. Haque, M.d.K. Zahan, Spectral and thermal characterization with antimicrobial activity on Cr (III) and Sn (II) complexes containing N, O Donor novel schiff base ligand, Intern. J. Chem. Stud. 4 (6) (2016) 08–11.
[9] P.A.M. Farias, M.B.R. Bastos, Electrochemical behavior of copper(ii) salen in aqueous phosphate buffer at the mercury electrode, Int. J. Electrochem. Sci. 4 (2009) 458–470.
[10] R.A. Khalil, A.H. Jalil, A.Y.A. Alrazzak, Application of a Schiff base derived from sulfanilamide as an acid-base indicator, J. Iran. Chem. Soc. 6 (2009) 345–352.
[11] K. Jamil, M. Bakhtiar, A.R. Khan, F. Rubina, R. Rehana, R. Wajid, M. Qaisar, A.F. Khan, A.K. Khan, M. Danish, M. Awais, Z.A. Bhatti, M. Rizwan, A. Naveed, M. Hussani, A. Pervez, Synthesis, characterization and antimicrobial activities of noval organotin compounds, Affr. J. Pure Appl. Chem. 3 (4) (2009) 66–71.
[12] G.G. Mohamed, M.M. Omar, A.M. Hindy, Metal complexes of schiff bases: preparation, characterization, and biological activity, Turk. J. Chem. 30 (2006) 361–362.
[13] Z.H. Chohan, S. Mushtaq, Zinc complexes of benzothiazole-derived schiff bases with antibacterial activity, J. Enz. Inhib. Med. Chem. 18 (3) (2003) 259–263.
[14] N.G.U. Sari, Antibacterial Activities of Some New Amino acid-Schiff, Bases J. Sci. 16 (2) (2003) 283–288.
[15] M.S. Islam, M.A Farooque, M.A.K. Bodruddoza, M.A. Mosaddik, M.S. Alam, Antimicrobial and Toxicological Studies of Mixed Ligand Transition Metal Complexes of Schiff Bases, J. Bio. Sci. 1 (8) (2001) 711–713.
[16] T.D. Thangadurai, S.K. Ihm, Chiral Schiff Base Ruthenium(III) Complexes: Synthesis, Characterisation, Catalytic and Antibacterial Studies, J. Ind. Eng. Chem. 9 (2003) 563-368.
[17] S. Baluja, A. Solanki, N. Kachhadia, Evaluation of biological activities of some Schiff bases and metal complexes, J. Iran. Chem. Soc. 3 (2006) 312–317.
[18] C. Spinu, M. Pleniceanu, C. Tigae, Biologically active transition metal chelates with a 2-Thiophenecarboxaldehyde-derived schiff base: synthesis, characterization, and antibacterial properties, Turk. J. Chem. 32 (2008) 487–493.
[19] T Kavitha, G Velraj, Molecular structure, spectroscopic and docking analysis of 1,3-diphenylpyrazole-4-propionic acid: a good prostaglandin reductase inhibitor, J. Mol. Struct. 1155 (2018) 819–830.
[20] N. Raman, V. Muthuraj, S. Ravichandran, A. Kulandaisamy, Synthesis, characterisation and electrochemical behaviour of Cu(II), Co(II), Ni(II) and Zn(II) complexes derived from acetylacetone andp-anisidine and their antimicrobial activity, Indi. J. Chem. Sci. 115 (2003) 161–167.

[21] V.S.V. Sathyanarayana, P. Sreevani, A. Sivakumar, V. Vijayakumar, Synthesis and antimicrobial activity of new Schiff bases containing coumarin moiety and their spectral characterization, ARKIVOC. (2008) 221–233 (xvii).
[22] A.D. Kulkarni, S.A. Patil, P.S. Badami, Electrochemical properties of some transition metal complexes: synthesis, characterization and in-vitro antimicrobial studies of Co(II), Ni(II), Cu(II), Mn(II) and Fe(III) Complexes, Ind. J. Electrochem. Sci. 4 (2009) 717–729.
[23] N. Raman, J.D. Raja, A. Sakthivel, Synthesis, spectral characterization of Schiff base transition metal complexes: DNA cleavage and antimicrobial activity studies, J. Chem. Sci. 119 (2007) 303–310.
[24] E. Racanska, O. Svajlenova, J. Valuska, J. Vanco, Antidiabetic Activity of Some Copper(ii) Schiff Base Complexes on Alloxan-induced Diabetic Mice, Acta Facul. Pharmac. Univer. Comen. Tomus LIII 53 (2006) 200–206.
[25] P.S. Chittilappilly, K.K.M. Yosuff, Synthesis, characterization and biological properties of ruthenium(III) Schiff base complexes derived from 3-hydroxyquinoxaline-2-carboxaldehyde, Indi. J. Chem. 47A (2008) 848–853.
[26] A. Cukurovali, I. Yilmaz, H. Ozmen, M. Ahamedzade, Schiff base ligands containing cyclobutane and their metal complexes with Co(II), Cu(II), Ni(II) and Zn(II) complexes of two novel Schiff base ligands and their antimicrobial activity, Trans. Met. Chem. 27 (2002) 171–176.
[27] M.J. Hearn, M.H. Cynamon, Design and synthesis of antituberculars: preparation and evaluation against Mycobacterium tuberculosis of an isoniazid Schiff base, J, Antimicrob. Chemoth. 53 (2004) 185–191.
[28] R. Nair, A. Shah, S. Baluja, S. Chanda, Synthesis and antibacterial activity of some Schiff base complexes, J. Serb. Chem. Soc. 71 (7) (2006) 733–744.
[29] N. Dharmaraj, P. Viswanathamurthi, K. Natarajan, Ruthenium(II) complexes containing bidentate Schiff bases and their antifungal activity, Trans. Met. Chem. 26 (2001) 105–109.
[30] A. Eşme, S.G. Sağdınç, Spectroscopic (FT-IR, FT-Raman, UV-Vis) analysis conformational, HOMO-LUMO, NBO and NLO calculations on monomeric and dimeric structures of 4-pyridazinecarboxylic acid by HF and DFT methods, J. Mol. Struct. 1147 (2017) 322–334.
[31] T.S. Rajan, M.V. Aanandhi, Molecular docking studies of isolated flavonoids compounds from Amaranthus tristis Linn. As alpha-amylase and alpha-glucosidase activators, Asian J. Pharm. Clin. Res. 10 (2018) 62–65.
[32] F. Shabani, L.A. Saghatforoush, S. Ghammamy, Synthesis, characterization and anti-tumour activity of iron(III) Schiff base complexes with unsymmetric tetradentate ligands, Bull. Chem. Soc. Elhiop 24 (2) (2010) 193–199.
[33] I. Sheikhshoaie, S. Saeednia, Synthesis, Characterization and Nonlinear Optical Properties of Four Novel Schiff Base Compounds, Arab. J. Sci.& Eng. 35 (2010) 53–60.
[34] W.T. Gao, Z. Zheng, Synthetic Studies on Optically Active Schiff-base Ligands Derived from Condensation of 2-Hydroxyacetophenone and Chiral Diamines, Molecules 7 (2002) 511–516.
[35] A. Faizul, S. Satendra, K.S. Lal, P. Om, Synthesis of Schiff bases of naphtha [1,2-d]thiazol-2-amine and metal complexes of 2-(2′-hydroxy)benzylideneam inonaphthothiazole as potential antimicrobial agents, J. Zhej. Univ. Sci. B. 8 (6) (2007) 446–452.
[36] M.N. Ibrahim, S.E.A. Sharif, Synthesis, Characterization and Use of Schiff Bases as Fluorimetric Analytical Reagents, E-J. Chem. 4 (2007) 531–535.
[37] K.B. Gudasi, G.S. Nadagouda, T.R. Goudar, Synthesis, characterization and biological studies of dioxouranium (II) and thorium (IV) complexes of Schiff bases derived from 2-aminopyridine and acetophenones, J. Ind. Chem. Soc. 83 (2006) 376–378.
[38] B.N. Muthal, Synthesis of new schiff bases and their transition metal complexes (CoII, NiII, CuI & ZnII) and their characterization stability constant and microbial activities, Pharm. Innov. J. 6 (3) (2017) 72–76.
[39] A.I. Vogel, in: Vogel's TextBook of Quantitative Chemical Analysis, fifth ed., Longmans, London, 1989, p. 233.
[40] Materials studio v 5.0, copyright Accelrys software Inc. (2009).
[41] W.J. Hehre, L. Radom, P.V.R. Schlyer, J.A. Pople, Ab Initio Molecular Orbital Theory, Wiley, New York, 1986.
[42] A. Kessi, B. Delley, Density functional crystal vs. cluster models as applied to zeolites, Inter. J. Quant. Chem. 68 (1998) 135–144.
[43] B. Hammer, L.B. Hansen, J.K. Norskov, Improved adsorption energetics within density-functional theory using revised Perdew-Burke-Ernzerhof functionals, Phy. Rev. B 59 (1999) 7413–7420.
[44] A. Matveev, M. Staufer, M. Mayer, N. Rosch, Density functional study of small molecules and transition-metal carbonyls using revised PBE functionals, Inter. J. Quant. Chem. 75 (1999) 863–873.
[45] S. Gautam, S. Chandra, H. Rajor, S. Agrawal, P.K. Tomar, Structural designing, spectral and computational studies of bioactive Schiff's base ligand and its transition metal complexes, Appl. Organometal Chem. 32 (2018) e3915.
[46] N.A. Ogorodnikova, J. Mol, Struct, THEOCHEM. 894 (2009) 41–49.
[47] L.J. Bellamy, in: The Infrared Spectra of Complex Molecules, Second ed., Chapman & Hall, Methuen, London, 1958, p. 274.
[48] J.R. Ferraro, in: Low-Frequency Vibrations of Inorganic and Coordination Compounds, Plenum press, New York, 1971, p. 308.
[49] K. Nakamoto, in: Infrared Spectra of Inorganic and Coordination Compounds, Part B, Fifth ed., Wiley Interscience, New York, 1971, p. 289.
[50] S. Roy, T.N. Mandal, K. Das, R.J. Butcher, A.L. Rheingold, S.K. Kar, Metal complexes of pyrimidine derived ligands–Syntheses, characterization and X-ray crystal structures of Ni (II), Co (III) and Fe (III) complexes of Schiff base ligands, J. Coord. Chem. 63 (2010) 2146–2157.
[51] S. Chandra, L.K. Gupta, EPR Electronic, magnetic and mass spectral studies of mono and homo-binuclear Co(II) and Cu(II) complexes with a novel macrocyclic ligand, Spectrochim. Acta 62A (2005) 1102–1106.
[52] P.P. Dholakiya, M.N. Patel, Metal Complexes, Preparation, Magnetic, Spectral, and Biocidal Studies of Some Mixed-Ligand Complexes with Schiff Bases Containing NO and NN Donor Atoms, Synth. React. Inorg. Mete. Org. Chem. 34 (2004) 553–563.
[53] R.A. Ammar, A.S. Alturiqi, A.M.A. Alaghaz, M.E. Zayed, Synthesis, spectral characterization, quantum chemical calculations, in-vitro antimicrobial and DNA activity studies of 2-(2′-mercaptophenyl) benzothiazole complexes, J. Mol. Struc. 1168 (2018) 250–263.
[54] G. Kalaiarasi, C. Umadevi, A. Shanmugapriya, P. Kalaivani, F. Dallemer, R. Prabhakaran, DNA (CT), protein (BSA) binding studies, anti-oxidant and cytotoxicity studies of new binuclear Ni (II) complexes containing 4 (N)-substituted thiosemicarbazones, Inorg. Chim. Acta. 453 (2016) 547–558.
[55] A. Kochem, G. Gellon, O. Jarjayes, C. Philouze, A.M. Hardemare, M. Gastel, F. Thomas, Nickel (II) radical complexes of thiosemicarbazone ligands appended by salicylidene, aminophenol and aminothiophenol moieties, Dalton Trans. 44 (2015) 12743–12756.
[56] A.Chakraborty Saswati, S.P. Dash, A.K. Panda, R. Acharyya, A. Biswas, S. Mukhopadhyay, S.K. Bhutia, A. Crochet, Y.P. Patil, M. Nethaji, R. Dinda, Synthesis, X-ray structure and in vitro cytotoxicity studies of Cu(i/ii) complexes of thiosemicarbazone: special emphasis on their interactions with DNA, Dalton Trans. 44 (2015) 6140–6157.
[57] R.J. Kunnath, M. Sithambaresan, A.A. Aravindakshan, A. Natarajan, M.R.P. Kurup, The ligating versatility of pseudohalides like thiocyanate and cyanate in copper (II) complexes of 2-benzoylpyridine semicarbazone: monomer, dimer and polymer, Polyhedron 113 (2016) 73–80.
[58] B.J. Hathaway, D.E. Billing, The electronic properties and stereochemistry of mono-nuclear complexes of the copper (II) ion, Coord. Chem. Rev. 5 (1970) 143–207.
[59] A.W. Coats, J.P. Redfern, Kinetic parameters from thermogravimetric data, Nature 20 (1964) 68–69.
[60] H.H. Horowitz, G. Metzger, A new analysis of thermogravimetric traces, Anal. Chem. 35 (1963) 1464–1468.
[61] G.O. Piloyan, T.D. Pyabonikar, C.S. Novikova, Determination of activation energies of chemical reactions by differential thermal analysis, Nature 212 (1966) 1229–1235.
[62] P.M. Maravalli, T.R. Goudar, Thermal studies of cobalt (II), nickel (II) and copper (II) 3-substituted-4-salicylideneamino-5-mercapto-1,2,4-triazole complexes, Thermochim. Acta 325 (1999) 95–105.
[63] K.K.M. Yusuff, R. Sreekala, Thermal and spectral studies of 1-benzyl-2- phenylbenzimidazole complexes of cobalt (II), Thermochim. Acta 159 (1990) 357–368.
[64] A.A. Frost, R.G. Pearson, Kinetics and Mechanism, Wiley, New York, 1961.
[65] L. Adrio, A.L. Demain, Microbial Enzymes, Tools for Biotechnological Processes, Biomolecules 4 (2014) 117–139.
[66] D. Sood, N. Kumar, V. Tomar, R. Chandra, Antibacterial and pharmacological evaluation of fluoroquinolones: a chemoinformatics approach, Genomics Inform. 16 (2018) 44–51.
[67] S. Sagdinc, B. Koksoy, F. Kandemirli, S.H. Bayari, Theoretical and spectroscopic studies of 5-fluoro-isatin-3-(N-benzylthiosemicarbazone) and its zinc (II) complex, J, Mol. Struct. 917 (2009) 63–70.